European Journal of Chemistry

View Journal Online
View Article Online

Synthesis, X-ray crystal structure, DFT, Hirshfeld surfaces, energy frameworks, and molecular docking analysis of a bicyclic ortho-aminocarbonitrile derivative

Ruchika Sharma [1], Sandeep Ashok Sankpal [2], Pradeep Jangonda Patil [2], Saminathan Murugavel [3], Sonachalam Sundramoorthy [4] and Rajni Kant [1,*]

[1] *Chemical Crystallography Laboratory, Department of Physics, University of Jammu, Jammu Tawi-180006, India*
[2] *Department of Chemistry, Shivaji University, Kolhapur, Maharashtra-416004, India*
[3] *Department of Physics, Thanthai Periyar Government Institute of Technology, Vellore-632002, Tamil Nadu, India*
[4] *Department of Physics, Agni College of Technology OMR, Thalambur, Chennai-600130, Tamil Nadu, India*

* *Corresponding author at: Chemical Crystallography Laboratory, Department of Physics, University of Jammu, Jammu Tawi-180006, India.*
e-mail: rkant.ju@gmail.com (R. Kant).

RESEARCH ARTICLE

10.5155/eurjchem.13.2.135-144.2225

Received: 21 January 2022
Received in revised form: 19 February 2022
Accepted: 20 February 2022
Published online: 30 June 2022
Printed: 30 June 2022

KEYWORDS

Hirshfeld surface
Molecular docking
X-ray crystallography
3D energy framework
Density functional theory
Molecular electrostatic potential

ABSTRACT

2-Amino-4-(2, 5-dimethoxyphenyl)-4a,5,6,7-tetrahydronaphthalene-1,3,3(*4H*)-tricarbonitrile has been synthesized and characterized by conventional spectroscopic techniques (FT-IR and ^{1}H NMR) and the three-dimensional structure elucidated by single crystal X-ray diffraction studies (SC-XRD). It exists in monoclinic crystal system with space group $P2_1/c$ and lattice parameters: a = 14.641(13) Å, b = 8.653(4) Å, c = 16.609(10) Å, β = 116.34(3)°, and Z = 4. In the crystal packing, molecules are connected through N-H···O and N-H···N intermolecular and intramolecular C-H···O interactions. The N1-H11···N2 interaction results in the formation of a dimer corresponding to $R_2^2(12)$ graph-set motif. The molecular structure has been theoretically optimized by using density functional theory (DFT) with the basis set B3LYP/6-311G (d,p). The optimized bond geometry shows consistency with the SC-XRD data. Besides this, the molecular electrostatic potential (MEP), Mulliken charges, and frontier molecular orbital analysis have been described. The d_{norm}, shape index, curvedness, crystal voids, 2D fingerprint (FP) plots, and 3D energy frameworks using Hirshfeld surface (HS) studies have also been computed and investigated. The molecular docking studies for 2-amino-4-(2, 5-dimethoxyphenyl)-4a,5,6,7-tetrahydronaphthalene-1,3,3(*4H*)-tricarbonitrile with DNA gyrase/lanosterol 14α-demethylase suggest that the compound may act as an active antimicrobial drug.

Cite this: *Eur. J. Chem.* **2022**, *13(2)*, 135-144 **Journal website**: www.eurjchem.com

1. Introduction

Ortho-aminocarbonitriles, comprising an important skeleton in organic synthesis, are a significant class of organic compounds [1,2]. Their derivatives are essential intermediates in various heterocyclic syntheses [3-6], exhibiting important optical properties [7,8] useful in artificial photosynthetic systems [9]. Such moieties, known as acceptor-donor-acceptor (A-D-A) systems [10], are key intermediates of various bioactive compounds [11]. Therefore, the synthesis of these compounds presents a key challenge in the development of newer synthetic reactions and pathways. The chemical synthesis of bicyclic ortho-amino carbonitrile derivatives is usually achieved via the Knoevenagel condensation and Michael addition under various conditions. Basic catalysts are traditionally used for this reaction, organic bases including pyrrolidine [3], piperidine [8], morpholine [12], imidazole [13], 1,4-diazabicyclo[2.2.2]octane [14,15], triethylamine [16,17] and ethane diamine [18] have been reported in the literature, and different types of ionic liquids have also been utilized for condensation [19-23].

The SC-XRD structure of 2-amino-4-(2, 5-dimethoxyphen yl)-4a, 5, 6, 7-tetrahydronaphthalene-1, 3, 3(*4H*)-tricarbonitrile (ADTNT) has been elucidated by X-ray diffraction methods and its optimized geometry computed using the B3LYP level of density function theory with 6-311G(d,p) basis set. The X-ray data in terms of bond distances and angles for ADTNT have been correlated with the structure optimized at B3LYP/6-311G (d,p) level. The Hirshfeld surface analysis was performed to visually portray the intermolecular interactions existing in the structure. Molecular docking study has been performed to understand the binding affinity of the molecule with DNA gyrase and lanosterol 14α-demethylase. The strong interaction of ligand and DNA gyrase [24] disturbs the biosynthesis of circular DNA in bacteria and it will induce bacterial death [25]. Due to this behavior, DNA gyrase (PDB id: 3G75) was chosen as the target for the antibacterial agent.

https://dx.doi.org/10.5155/eurjchem.13.2.135-144.2225

Table 1. Crystal data and structure refinement for ADTNT.

CCDC number	2132239
Empirical formula	$C_{21}H_{20}N_4O_2$
Formula weight	361.42
Temperature (K)	293(2)
Crystal system	Monoclinic
Space group	$P2_1/c$
a, (Å)	14.641(13)
b, (Å)	8.653(4)
c, (Å)	16.609(10)
α (°)	90.00
β (°)	116.34(3)
γ (°)	90.00
Volume (Å^3)	1886(2)
Z	4
ρ_{calc} (g/cm^3)	1.273
μ (mm^{-1})	0.084
F(000)	764.0
Crystal size (mm^3)	0.40 × 0.30 × 0.20
Radiation	MoKα (λ = 0.71073)
2Θ range for data collection (°)	5.64 to 47.98
Index ranges	$-16 \le h \le 16$, $-9 \le k \le 9$, $-19 \le l \le 18$
Reflections collected	31296
Independent reflections	2888 [R_{int} = 0.1593, R_{sigma} = 0.0721]
Data/restraints/parameters	2888/0/255
Goodness-of-fit on F^2	1.092
Final R indexes [I≥2σ (I)]	R_1 = 0.0963, wR_2 = 0.2494
Final R indexes [all data]	R_1 = 0.1297, wR_2 = 0.2697
Largest diff. peak/hole (e.Å^{-3})	0.34/-0.26

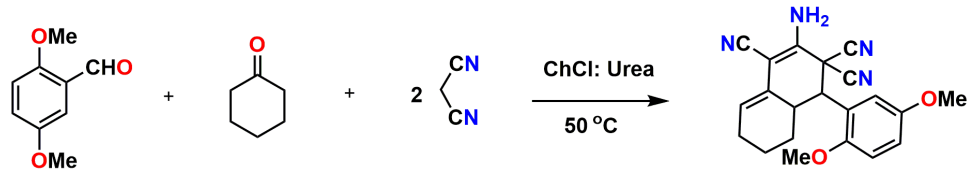

Scheme 1. Synthesis of 2-amino-4-(2,5-dimethoxyphenyl)-4a,5,6,7-tetrahydronaphthalene-1,3,3(*4H*)-tricarbonitrile (ADTNT).

Lanosterol 14α-demethylase [26] enzyme controls the production of ergosterol and is most important for the fungal growth and survival [27]. Thus, Lanosterol 14α-demethylase (PDB id: 1EA1) has been chosen as an antifungal agent target. In addition, the docking results of the ADTNT have been compared with those of the conventional medicines, ciprofloxacin (Bacteria) and fluconazole (Fungi).

2. Experimental

2.1. Synthesis

A three component reaction of 2,5-dimethoxy benzaldehyde (**1**) (0.106 g), cyclohexanone (**2**) (0.098 g) and malononitrile (**3**) (0.132 g) was heated at 50 °C in choline chloride:urea deep eutectic solvent (ChCl:Urea DES) (0.5 mL) until the completion of the reaction, tested by thin-layer chromatography (TLC) [28]. After completion of the reaction, 5 mL water was added to the crude precipitate and the product was filtered and recrystallized from hot ethanol to have pure ortho-aminocarbonitrile derivative **4**. The schematic diagram of the synthesized compound is shown in Scheme 1. 2-Amino-4-(2, 5-dimethoxyphenyl)-4a, 5, 6, 7-tetrahydronaphthalene-1, 3, 3(*4H*)-tricarbonitrile (**ADTNT**): Yield: 85%. Time: 20 min. Color: Yellow. M.p.: 218-220 °C. Ft-IR (KBr, ν, cm^{-1}): 714, 806, 1029, 1213, 1278, 1459, 1506, 1643, 1700, 2207, 2322, 2360, 2838, 2935, 3122, 3329, 3434, 3447. ^{1}H NMR (400 MHz, DMSO-d_6, δ, ppm): 0.83 (1H, m, CH_2), 1.35 (1H, m, CH_2), 1.65-1.55 (2H, m, CH_2), 2.04-2.03 (1H, d, CH_2), 2.15-2.11 (1H, d, CH_2), 2.59 (1H, d, CH_2), 3.65 (3H, s, -OCH_3), 3.69 (3H, s, OCH_3), 3.83 (1H, m, methine), 5.77 (1H, s, olefinic), 6.22 (2H, s, -NH_2), 6.79 (1H, d, Ar-H), 6.83 (1H, d, Ar-H), 6.94-6.96 (1H, d, Ar-H).

2.2. X-ray structure determination

A single-crystal X-ray diffraction experiment for the structure elucidation of ADTNT has been performed on a Bruker D8 Venture diffractometer using MoKα radiation (λ = 0.71073 Å). The intensities were recorded in ϕ and ω-scan mode over a range of diffraction angles (2.82-23.99°). The reflection data were treated by using the standard criteria to obtain 1973 as the observed reflections and the same were corrected for various factors. The structure has been solved by direct methods using SHELXS97 [29] and refined anisotropically by full-matrix least-squares using SHELXL97 [30]. All non-H atoms were refined anisotropically and the final refinement cycle yielded a final *R* = 0.0963 and *w*R(F^2) = 0.2494 for 1973 observed reflections. The atomic scattering coefficients were derived from the International Tables for X-ray Crystallography (1992, Vol. C, Tables 4.2.6.8 and 6.1.1.4) [31]. The crystal and structure refinement data are presented in Table 1. The geometry of the molecule has been analyzed using MERCURY [32], PLATON [33] and PARST [34] software.

2.3. Computational methodology

The optimized structure was obtained using quantum mechanical calculations (Gaussian 09W software package [35]) followed by the functional B3LYP with 6-311G(d,p) basis set. The SC-XRD parameters were compared with the ones obtained theoretically. Some other properties, such as, Molecular Electrostatic Potential (MEP), Mulliken charges and HOMO-LUMO energy gap were also investigated. The Molecular Hirshfeld surfaces (HSs), fingerprint plots (FPs), and crystal voids evaluation, being the unique tools for determining the properties of a crystal structure, have been performed using Crystal Explorer program (version 21.5) [36]).

Table 2. Experimental and theoretical bond lengths and angles for ADTNT.

Parameters	B3LYP/6-311G(d,p)	XRD	Parameters	B3LYP/6-311G(d,p)	XRD
Bond lengths (Å)			**Bond angles (°)**		
C3-O1	1.365	1.377(5)	O1-C3-C4	125.2	124.2(4)
C8-O1	1.419	1.421(6)	O1-C3-C2	115.6	116.8(3)
C6-O2	1.369	1.374(5)	O2-C6-C5	124.0	125.2(4)
C7-O2	1.421	1.422(5)	O2-C6-C1	116.2	114.5(4)
C18-C21	1.477	1.489(5)	C2-C1-C9	122.1	122.2(3)
C21-N4	1.152	1.131(5)	C6-C1-C9	119.2	119.8(4)
C18-C20	1.477	1.489(6)	C17-C16-C19	116.2	117.8(4)
C20-N3	1.152	1.138(6)	C19-C16-C15	119.2	117.8(3)
C17-N1	1.364	1.361(6)	N1-C17-C18	115.6	114.8(3)
C16-C19	1.426	1.433(6)	C16-C17-N1	124.5	124.8(4)
C19-N2	1.157	1.150(5)	C17-C18-C21	109.2	110.6(3)
C9-C1	1.519	1.529(5)	C17-C18-C20	107.3	106.1(3)
C15-C10	1.523	1.513(6)	C1-C9-C18	111.7	110.2(3)
C14-C15	1.344	1.331(6)	C20-C18-C9	111.9	111.5(3)
C16-C17	1.366	1.356(6)	C21-C18-C9	109.4	108.4(3)

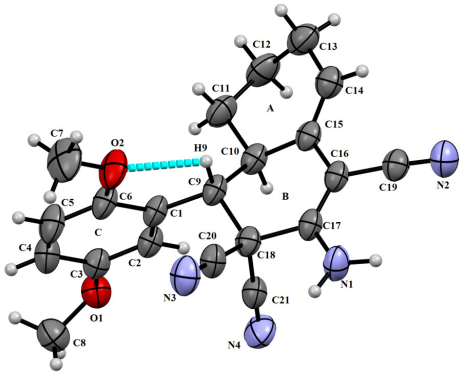

Figure 1. The ORTEP diagram of the molecule with atomic labelling (40% ellipsoidal probability).

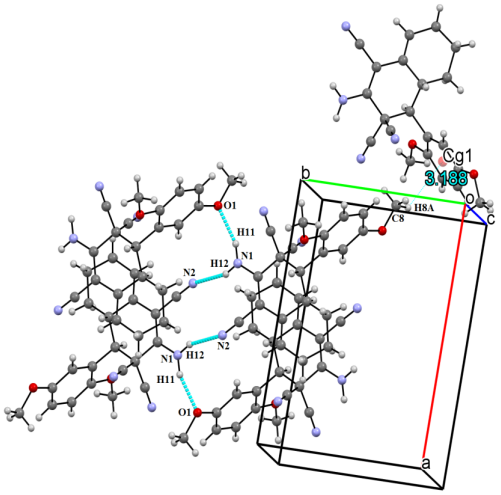

Figure 2. Hydrogen bonding interactions showing a dimer (R_2^2 (12) graph set motif).

The B3LYP/6-311G(d,p) energy model has been used to compute various intermolecular interaction energies as well as the total interaction energy between the molecules. The binding affinity has been determined by docking the molecule into the active site of the target protein. The AutoDock Vina software [37] has been used to analyze the docking modes of the molecule into the active site of the target protein structure. The target protein DNA gyrase and enzyme Lanosterol 14 α-demethylase were imported from the protein data bank (www.rcsb.org/pdb). The grid center is fixed at X = 51.19, Y = -3.99, Z = 17.94 (for DNA gyrase) and X = -17.28, Y = -7.28, Z = 63.72 (for lanosterol-14α-demethylase) for docking purpose. Discovery Studio Visualizer is used to modeled and visualized the stabilized complex structures.

3. Results and discussion

3.1. Structural and molecular geometry analysis

An ORTEP plot of the molecular structure containing the atom numbering scheme (thermal ellipsoid drawn at 40% probability level) is depicted in Figure 1. Some selected bond distances and bond angles are presented in Table 2. The rings have been labeled as A, B, and C. The ring A is fused with ring - B through the bond C10-C15 = 1.513 Å and this value is quite similar to literature for some analogous structures [38,39]. It adopts half-chair conformation, with two-fold rotation axis bisecting the bond C11-C12 (ΔC_2 (C11-C12) = 0.49).

Table 3. Hydrogen bond lengths (Å) and angles (°) for ADTNT *.

D-H···A	D-H	H···A	D···A	∠D-H···A
N1-H11···O1 [i]	0.94(6)	2.04(6)	2.925(6)	158(4)
N1-H12···N2 [ii]	0.91(5)	2.28(5)	3.135(7)	156(5)
C9-H9···O2	0.98	2.24	2.738(5)	110
C8-H8···Cg1 [iii]	0.96	3.19	3.856(7)	128.2

* Symmetry code: i) *x*, 1+*y*, *z*; ii) 1-*x*, 3-*y*, 1-*z*; iii) –*x*, -1/2+*y*, 1/2+*z*. Cg1: C1/C2/C3/C4/C5/C6.

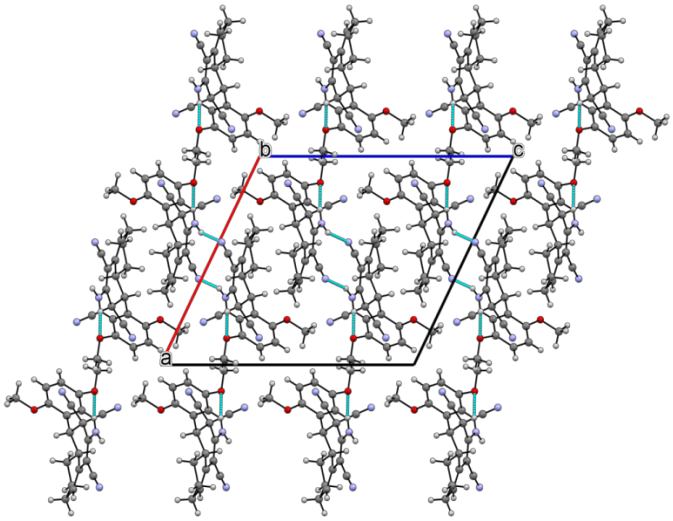

Figure 3. Packing arrangement of molecules along the *b* axis.

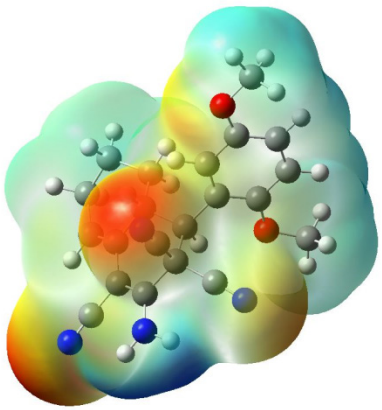

Figure 4. Molecular electrostatic potential map of ADTNT.

The ring B adopts a chair conformation with best mirror plane passing through the atoms C16 and C17, respectively, the asymmetric parameters being: ΔC_S (C16) = 0.346 Å and ΔC_S(C17) = 0.346 Å, and the best two-fold rotation axis bisects the bonds C8-C9 and C10-C15 (ΔC_2(C8-C9) = 0.212 and ΔC_2(C10-C15) = 0.212 Å. The ring C is essentially planar with a maximum deviation of 0.0074 Å (C6). The optimized geometrical parameters (bond length and bond angles) have been computed using DFT method by employing 6-311G(d,p) basis set (Table 2) where it may be observed that the SC-XRD and optimized parameters are in agreement within the limits of experimental errors. There are two intermolecular interactions (N1-H11···O1, N1-H12···N2) of which the N1-H12···N2 results in the formation of a dimer with a $R_2^2(12)$ graph set motif (Figure 2). Besides this, there exists one C9-H9···O2 intramolecular and one C-H···π interaction. A summary of intra- and inter-molecular hydrogen bonding is given in Table 3. Packing of molecules in the unit cell as viewed along *b*-axis is shown in Figure 3.

3.2. Computational details

3.2.1. Molecular electrostatic potential and Mulliken charge analysis

The molecular electrostatic potential (MEP) map is a useful tool for explaining the electrostatic interactions [40]. In order to find the most active regions of the molecule, the molecular electrostatic potential map and Mulliken charges were taken into consideration. The negative area, which is considered a nucleophilic site, is usually colored red (the strongest repulsion), whereas the negative region, which is the preferred electrophilic site, is colored blue (strongest attraction). The green-colored patch on the map shows a neutral potential. From the MEP map as shown in Figure 4, it is evident that most of the reactive and negative region is around the cyanide group. The electrons present in this area could be readily provided to the acceptor species. In addition, the most positive area is located on the hydrogen atoms of the amino group.

Table 4. Mulliken charge values of ADTNT.

Atom	Charge	Atom	Charge
N1	-0.451	H1A	0.236
N2	-0.232	H1B	0.238
N3	-0.213	H2	0.112
N4	-0.208	H4	0.105
O1	-0.348	H5	0.106
O2	-0.381	H7A	0.108
C1	-0.133	H7B	0.131
C2	-0.050	H7C	0.120
C3	0.169	H8A	0.112
C4	-0.121	H8B	0.132
C5	-0.111	H8C	0.107
C6	0.239	H9	0.173
C7	-0.129	H10	0.146
C8	-0.132	H11A	0.114
C9	-0.105	H11B	0.129
C10	-0.171	H12A	0.115
C11	-0.172	H12B	0.114
C12	-0.227	H13A	0.123
C13	-0.173	H13B	0.121
C14	-0.108	H14	0.106
C15	-0.027		
C16	0.098		
C17	0.232		
C18	-0.256		
C19	-0.016		

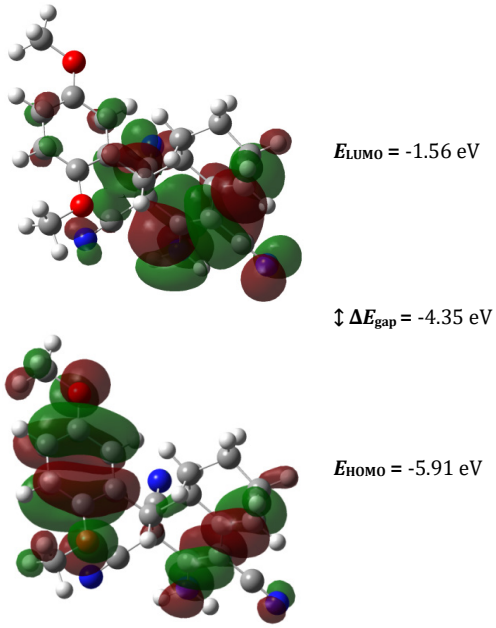

Figure 5. Surface plots of HOMO and LUMO.

The calculated Mulliken charges (Table 4) were used to investigate the reactive sites of the molecule and it is observed that all carbon atoms except C3 (0.169), C6 (0.239), C16 (0.098) and C17 (0.232) possess negative charges while the hydrogen atoms exhibit positive Mulliken charge values. The atom N1 (-0.451) possesses the highest negative charge value and thus results in the formation of N1-H11···O1 and N1-H12···N2 intermolecular contacts.

3.2.2. Frontier molecular orbital analysis

The investigation of frontier molecular orbitals explains the single-electron excitation from HOMO to LUMO. The energy difference between HOMO (acts as an electron donor) and LUMO (acts as an electron acceptor) describes the eventual charge transfer interaction within the molecule. All parameters such as energy levels, energy gaps, electron affinity, the ionization potential, etc. are presented in Table 5. The transition of the electron from the HOMO to the LUMO energy levels is shown in Figure 5. A molecule with a small HOMO-LUMO energy gap (soft molecules) has low kinetic stability and high chemical reactivity, while in the case of a large energy gap; it is assumed to be a hard molecule with low chemical reactivity. Thus, based on the data as collated and presented in Table 5, it may be assumed as a hard molecule having a HOMO-LUMO energy gap of 4.35 eV.

3.2.3. Hirshfeld surface analysis

The study of HSs and FPs obtained by the Crystal Explorer (21.5) program is one of the most recent techniques for assessing intermolecular interactions in the crystal phase and these are obtained by taking the data of SC-XRD structure as input. The HS allows to view the molecular contacts that are important in the self-assembly of a crystal. It is also measured by comprehensive two-dimensional fingerprint plots, which

Table 5. HOMO-LUMO and global reactivity descriptor values of ADTNT.

Property	Symbols and formula	Value (eV)
HOMO energy	E_H	-5.91
LUMO energy	E_L	-1.56
Energy gap	$E_{g1} = (E_H - E_L)$	4.35
Chemical hardness (η)	$\eta = (E_L - E_H)/2$	2.17
Global softness (σ)	$\sigma = 1/2\eta$	0.23
Chemical potential (μ)	$\mu = (E_L + E_H)/2$	-3.73
Electronegativity (χ)	$\chi = -\mu$	3.73
Electrophilicity (ω)	$\mu^2/2\eta$	3.20

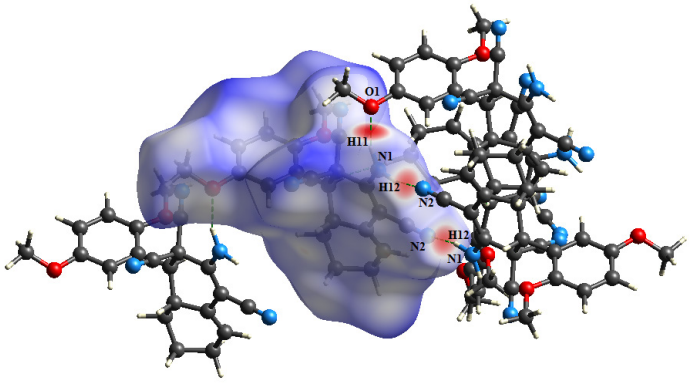

Figure 6. Front view of 3D d_{norm} surface (HS).

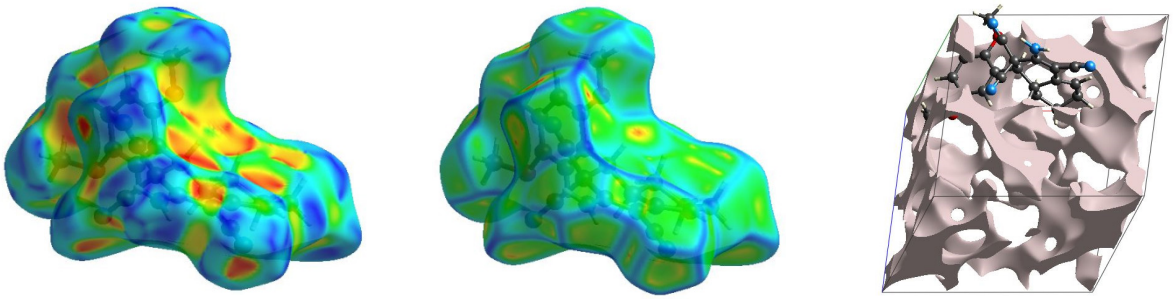

(a) (b) (c)

Figure 7. (a) Shape index map, (b) curvedness map, and (c) crystal voids (using (0.002 au) - isosurface).

indicate the contribution of each interaction to the entire HS of the molecule and provide a three-dimensional image showing close contacts in the crystal, which may be summed up in a fingerprint plot. Figure 6 shows the d_{norm} surface mapped over the range of -0.4933 to 1.6054 a.u. The d_{norm} surface represents many red spots of numerous sizes and intensities, indicating the presence of dominant interactions containing the donor and acceptors. The interaction between the hydrogen atom of amine group and its adjacent nitrogen atom (N1-H12···N2) forms a dimer (Figure 6). There exists another red spot on the HS indicating an intermolecular contact N1-H11···O1.

Figure 7a shows the shape index map produced within the range -1 to 1 Å. The convex blue portions indicate hydrogen donor groups, whereas the concave red parts represent hydrogen acceptor groups. The nonexistence of contiguous red and blue triangles on the shape-index plot indicates the absence of π-π interactions. The curvedness map, generated in the range -4.0 to 4.0 Å, as shown in Figure 7b, depicts enormous areas of green with no flat (i.e. planar) surface area, whereas the blue patches show areas of curvature. The voids, as shown in the crystal structure (Figure 7c), have been found by building a (0.002 au) - isosurface of procrystal electron density. This isosurface is further used to calculate the empty space by identifying the shape (form) and size of the molecules. This gives the void volume as 464.13 Å^3. With a unit cell volume of 1886(2) Å^3 (Table 1), the approximated void volume is 24.6% of the entire unit cell volume.

The overall two-dimensional FPs with contacts divided into H···H, H···O/O···H, H···C/C···H, H···N/N···H, O···N/N···O, N···N, and C···N/N···C, with their respective contributions to the HS are shown in Figure 8. The H···H interactions, accounting for 38.9% of the total crystal packing, are the most significant intermolecular interactions. The H···N/N···H interactions resulting from intermolecular N-H···N hydrogen bonding contribute 33.9% to the HS and are represented by a pair of strong spikes in the area $d_e + d_i \sim 2.6$ Å (Figure 8). The pair of wings in the FP plots demarcated into H···C/C···H contacts contribute 19.2% to the HS, have a roughly symmetrical distribution of points (with $d_e + d_i \sim 2.69$ Å). Similarly, H···O/O···H contributes 6.2% to the HS.

3.2.4. Energy framework analysis

The B3LYP/6-311G(d,p) energy model (as available in Crystal Explorer 21.5) has been employed for the computation of various intermolecular interaction energies as well as the total interaction energy between the molecules. The total interaction energy (E_{tot}) of the molecule is the sum of its classical electrostatic/coulomb energy (E_{ele}), polarization energy (E_{pol}), dispersion energy (E_{disp}), and exchange repulsion energy (E_{rep}) along with their scale factors of 1.057, 0.740, 0.871, and 0.618, respectively [41].

Table 6. Different interaction energies of the molecular pairs in kJ/mol.

N	Symmetry operation	Centroid distance (R)	Electron density	E_{ele}	E_{pol}	E_{dis}	E_{rep}	E_{tot}
1	-x, -y, -z	12.25	B3LYP/6-31G(d,p)	3.2	-0.6	-7.1	0.0	-3.3
1	-x, -y, -z	9.75	B3LYP/6-31G(d,p)	-10.0	-2.2	-12.9	3.0	-21.6
2	x, -y+1/2, z+1/2	8.89	B3LYP/6-31G(d,p)	-6.0	-1.8	-14.8	7.4	-16.1
2	-x, y+1/2, -z+1/2	9.60	B3LYP/6-31G(d,p)	-6.3	-1.6	-23.2	15.0	-18.8
1	-x, -y, -z	7.04	B3LYP/6-31G(d,p)	-12.7	-6.3	-68.1	44.9	-49.7
2	-x, y+1/2, -z+1/2	7.56	B3LYP/6-31G(d,p)	-6.1	-1.8	-45.6	19.7	-35.3
2	x, y, z	8.65	B3LYP/6-31G(d,p)	-32.0	-8.4	-31.4	40.6	-42.3
2	x, -y+1/2, z+1/2	9.95	B3LYP/6-31G(d,p)	3.2	-0.8	-5.3	0.8	-1.2
1	-x, -y, -z	12.01	B3LYP/6-31G(d,p)	-48.8	-9.7	-11.2	0.0	-68.6

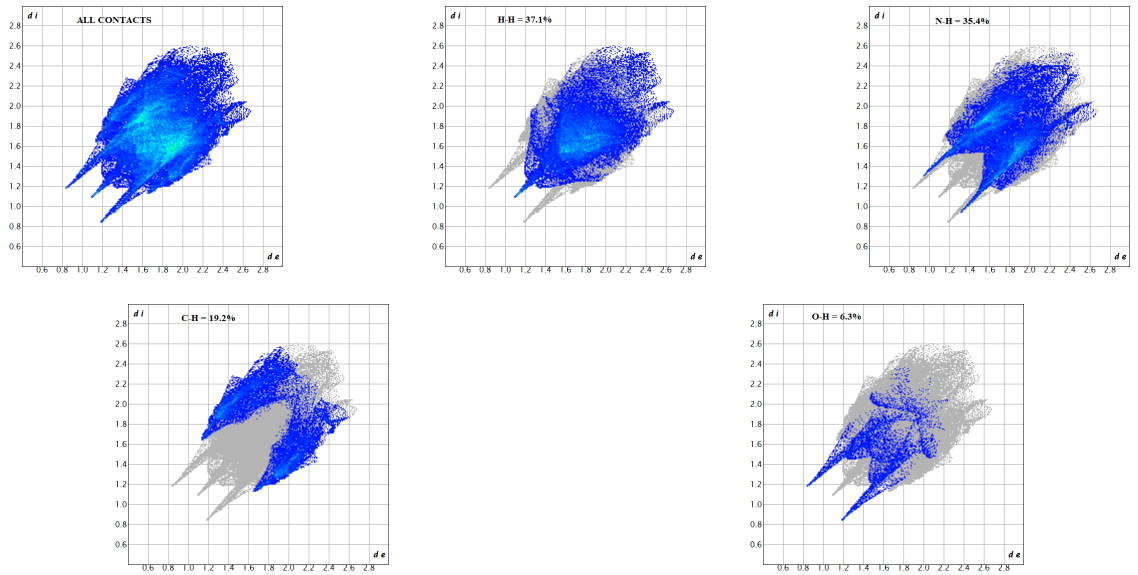

Figure 8. Two-dimensional fingerprint plots showing the percentage of contacts that contribute to the total Hirshfeld surface area of the molecule.

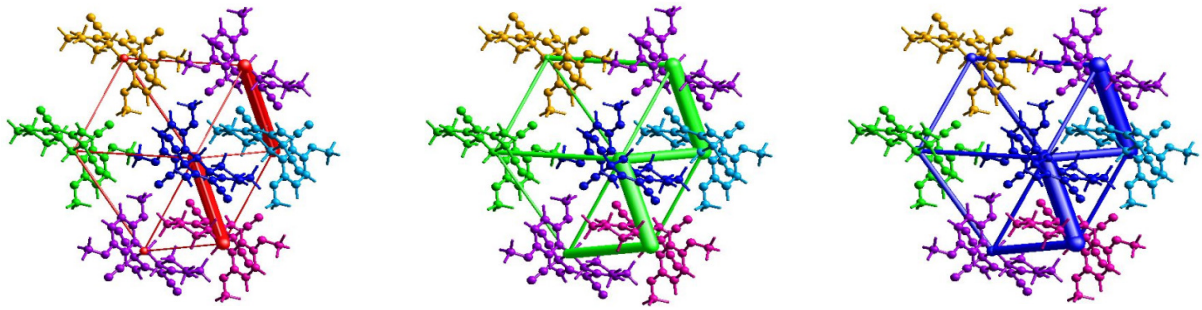

(a) (b) (c)

Figure 9. The graphical representation of energy frameworks along *b*-axis: (a) coulomb interaction energy (red), (b) dispersion interaction energy (green) and (c) total interaction energy (blue). To make the figure clear, the inconsiderable contacts weaker than the threshold energy (10 kcal/mol) have been neglected.

The cylinder-shaped energy frameworks represent the relative strength in the interaction energies and also provide information on their role in the stabilization of the crystal packing (Figure 9). From Table 6, it is quite evident that the dispersion force plays a dominant role, having a maximum energy of -219.6 kJ/mol, while the total interaction energy is -256.9 kJ/mol.

3.2.5. Molecular docking analysis

The ADTNT-DNA gyrase complex is stabilized by eight hydrogen interactions with residues ASN54, VAL130, VAL131, GLU50, and ASP57 as shown in Figure 10a. The binding energy, bond length, and bonding type of interaction in complex ADTNT-DNA gyrase were listed in Table 7. The docking output predicts that the binding affinity of ADTNT-DNA gyrase complex (-7.10 kcal/mol) has comparatively a better binding energy score when compared with Ciprofloxacin-DNA gyrase complex (-4.01 kcal/mol) [42]. The ADTNT-Lanosterol 14α-demethylase complex is stabilized by six hydrogen interactions with residues GLN72, ARG96, and GLY388 as shown in Figure 12b and the binding energy, bond length, and bonding type of interaction in this complex is given in Table 7.

Table 7. Binding energy, hydrogen bonds of ADTNT with DNA gyrase and lanosterol 14α-demethylase *.

Complex	Binding energy, kcal/mol	Interactions	Distance, Å	Bonding	Bonding types
1	7.1	ASN54[HD1···N]	2.4273	Hydrogen	H-bond
		VAL130[HN···N]	2.7370	Hydrogen	H-bond
		VAL131 [HN···N]	1.9723	Hydrogen	H-bond
		[H···OD2]GLU50	2.2090	Hydrogen	H-bond
		[H···O]ASN54	2.6585	Hydrogen	H-bond
		[C···OE1]GLU50	3.5240	Hydrogen	CH-bond
		[C···OE2]GLU50	3.5563	Hydrogen	CH-bond
		[C···OD1]ASP57	3.6520	Hydrogen	CH-bond
2	8.8	GLN72[HE1···N]	2.4103	Hydrogen	H-bond
		ARG96[HE···N]	2.0905	Hydrogen	H-bond
		ARG96[HE···N]	3.0661	Hydrogen	H-bond
		[H···OE1]GLN72	2.6582	Hydrogen	H-bond
		[H···OE1]GLN72	2.8737	Hydrogen	H-bond
		MET79[SD···π]	3.5516	Other	Pi-Sulfur

* 1 = ADTNT + DNA gyrase; 2 = ADTNT + Lanosterol 14α-demethylase.

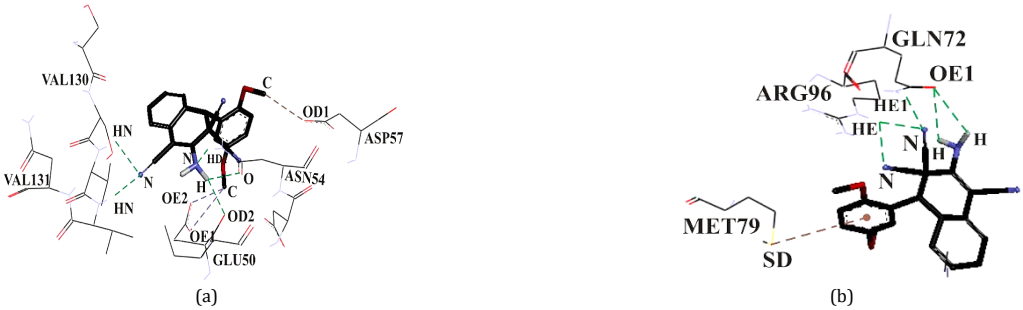

(a) (b)

Figure 10. Molecular interaction of ADTNT with (a) DNA gyrase and (b) Lanosterolo 14α-demethylase binding sites.

The docking output predicts that the binding affinity of ADTNT-Lanosterol 14α-demethylase complex (-8.80 kcal/mol) is almost twice the binding energy score as in the case of Fluconazole-Lanosterol 14α-demethylase complex (-3.59 kcal/mol) [42]. The ADTNT reveals a strong binding interaction with the targets (DNA gyrase/Lanosterol 14α-demethylase) and have more docking affinity score than the standard drugs (Ciprofloxacin and fluconazole). Hence, it may act as an active anti-microbial (antibacterial and antifungal) drug.

4. Conclusions

In this paper, the synthesis, SC-XRD structure and characterization of 2-amino-4-(2,5-dimethoxyphenyl)-4a,5,6,7-tetrahydronaphthalene-1,3,3(*4H*)-tricarbonitrile using available computational tools have been reported. The structure exists in the monoclinic crystal system and the molecule is stabilized by N-H···N and N-H···O intermolecular and C-H···O intramolecular hydrogen bonds. The N1-H11···N2 interaction results in the formation of a dimer (with a $R_2^2(12)$ graph set motif). The optimized structure has been compared with the SC-XRD data and with some related structures as well. The MEP map shows that the cyanide group is the most negative region whereas the most positive area is situated on the hydrogen atoms of the amino group. The HOMO-LUMO energy gap of 4.359 eV makes it a hard molecule with low chemical reactivity and high kinetic stability. HS and two-dimensional FP plots show that the molecular structure is stabilized through many intermolecular contacts such as H···H, H···O/O···H, H···C/C···H, and H···N/N···H contacts. The estimated void volume of the molecule is 24.6% of the unit cell volume. The energy framework analysis indicates that the dispersion energy is quite dominant (-219.6 kJ/mol) when compared with the total interaction energy (-256.9 kJ/mol). The molecular docking analysis reveals that the ADTNT molecule possesses high binding affinity when compared with some standard drugs and it may thus be a step towards finding a new and improved antimicrobial agent.

Acknowledgements

Rajni Kant thanks the University of Jammu for funding under the RUSA- 2.0 project of the Government of India.

Supporting information

CCDC-2132239 contains the supplementary crystallographic data for this paper. These data can be obtained free of charge via https://www.ccdc.cam.ac.uk/structures/, or by e-mailing data request@ccdc.cam.ac.uk, or by contacting The Cambridge Crystallographic Data Centre, 12 Union Road, Cambridge CB21EZ, UK; fax:+44(0)1223-336033.

Disclosure statement

Conflict of interest: The authors declare that they have no conflict of interest.
Ethical approval: All ethical guidelines have been adhered.
Sample availability: Sample of the compound is available from the author

CRediT authorship contribution statement

Conceptualization: Ruchika Sharma; Methodology: Ruchika Sharma, Rajni Kant; Software: Ruchika Sharma; Synthesis (FTIR, 1H NMR): Sandeep Ashok Sankpal, Pradeep Jangonda Patil; Formal Analysis: Ruchika Sharma, Rajni Kant; Investigation: Ruchika Sharma, Rajni Kant; Resources: Rajni Kant; Data Curation (Molecular docking): Saminathan Murugavel, Sonachalam Sundramoorthy; Writing - Original Draft: Rajni Kant; Writing - Review and Editing: Ruchika Sharma; Visualization: Rajni Kant; Supervision: Rajni Kant; Project Administration: Rajni Kant.

ORCID and Email

Ruchika Sharma
ruchi18nik@gmail.com
https://orcid.org/0000-0002-5698-4067
Sandeep Ashok Sankpal
sandeeporg1@gmail.com
https://orcid.org/0000-0001-8209-5899
Pradeep Jangonda Patil
patilpradeep197@gmail.com
https://orcid.org/0000-0002-2880-8226

Saminathan Murugavel
smurugavel27@gmail.com
https://orcid.org/0000-0002-4626-8104
Sonachalam Sundramoorthy
sunphysics17@gmail.com
https://orcid.org/0000-0002-5310-0692
Rajni Kant
rkant.ju@gmail.com
https://orcid.org/0000-0001-8043-2329

References

[1]. Enders, D.; Hüttl, M. R. M.; Grondal, C.; Raabe, G. Control of four stereocentres in a triple cascade organocatalytic reaction. *Nature* **2006**, *441*, 861–863.
[2]. Padwa, A. Domino reactions of rhodium(II) carbenoids for alkaloid synthesis. *Chem. Soc. Rev.* **2009**, *38*, 3072–3081.
[3]. Mojtahedi, M. M.; Pourabdi, L.; Abaee, M. S.; Jami, H.; Dini, M.; Halvagar, M. R. Facile one-pot synthesis of novel ortho-aminocarbonitriles and dicyanoanilines fused to heterocycles via pseudo four-component reactions. *Tetrahedron* **2016**, *72*, 1699–1705.
[4]. Rong, L.; Tao, S.; Xia, S.; Liu, L.; Yin, S.; Shi, Y. An efficient synthesis of 2-amino-4-aryl-6,7,8,9-tetrahydro-5H-benzo[7]annulene-1,3-dicarbonitriles in THF with DBU as catalyst. *Res. chem. intermed.* **2012**, *38*, 1647–1654.
[5]. Shabalala, N. G.; Maddila, S.; Jonnalagadda, S. B. Facile one-pot green synthesis of tetrahydrobiphenylene-1,3-dicarbonitriles in aqueous media under ultrasound irradiation. *Res. chem. intermed.* **2016**, *42*, 8097–8108.
[6]. Abaee, M. S.; Ehteshami, F.; Forghani, S.; Mojtahedi, M. M.; Hadizadeh, A. Facile one-pot synthesis of novel dicyanoanilines fused to dithiane ring via a pseudo-four-component reaction. *J. Iran. Chem. Soc.* **2017**, *14*, 1151–1157.
[7]. Cui, S.-L.; Lin, X.-F.; Wang, Y.-G. Parallel synthesis of strongly fluorescent polysubstituted 2,6-dicyanoanilines via microwave-promoted multicomponent reaction. *J. Org. Chem.* **2005**, *70*, 2866–2869.
[8]. Sepioł, J.; Milart, P. Elimination of the nitrile group from o-aminonitriles—IV. *Tetrahedron* **1985**, *41*, 5261–5265.
[9]. Kurreck, H.; Huber, M. Modellreaktionen für die Photosynthese – photoinduzierter Ladungs- und Energietransfer zwischen verknüpften Porphyrin- und Chinon-Einheiten. *Angew. Chem. Weinheim Bergstr. Ger.* **1995**, *107*, 929–947.
[10]. Moshtaghi Zonouz, A.; Eskandari, I.; Notash, B. An efficient and green procedure for the synthesis of highly substituted polyhydronaphthalene derivatives via a one-pot, multi-component reaction in aqueous media. *Curr. Chem. Lett.* **2015**, 85–92.
[11]. Singh, F. V.; Vatsyayan, R.; Roy, U.; Goel, A. Arylanthranilodinitriles: a new biaryl class of antileishmanial agents. *Bioorg. Med. Chem. Lett.* **2006**, *16*, 2734–2737.
[12]. Elinson, M. N.; Ilovaisky, A. I.; Merkulova, V. M.; Barba, F.; Batanero, B. General approach to spiroacenaphthylene pentacyclic systems: direct multicomponent assembling of acenaphthenequinone and cyclic carbonyl compounds with two molecules of malononitrile. *Tetrahedron* **2013**, *69*, 7125–7130.
[13]. Ghosh, K.; Kar, D.; Panja, S.; Bhattacharya, S. Ion conducting cholesterol appended pyridinium bisamide-based gel for the selective detection of Ag+and Cl−ions. *RSC Adv.* **2014**, *4*, 3732–3737.
[14]. Chinchkar, S. M.; Patil, J. D.; Korade, S. N.; Gokavi, G. S.; Shejawal, R. V.; Pore, D. M. DABCO: An efficient catalyst for pseudo multi-component reaction of cyclic ketone, aldehyde and malononitrile. *Lett. Org. Chem.* **2017**, *14*(6), 403–408.
[15]. Yan, S.; Dong, D.; Xie, C.; Wang, W.; Wang, Z. Synthesis of bicyclic ortho-aminocarbonitrile derivatives catalyzed by 1,4-diazabicyclo [2.2.2]octane. *Youji huaxue* **2019**, *39*, 2560–2566.
[16]. Hari Babu, T.; Abragam Joseph, A.; Muralidharan, D.; Perumal, P. T. A novel method for the synthesis of functionalized spirocyclic oxindoles by one-pot tandem reaction of vinyl malononitriles with isatylidene malononitriles. *Tetrahedron Lett.* **2010**, *51*, 994–996.
[17]. Elinson, M. N.; Vereshchagin, A. N.; Nasybullin, R. F.; Bobrovsky, S. I.; Ilovaisky, A. I.; Merkulova, V. M.; Bushmarinov, I. S.; Egorov, M. P. General approach to a spiro indole-3,1′-naphthalene tetracyclic system: stereoselective pseudo four-component reaction of isatins and cyclic ketones with two molecules of malononitrile. *RSC Adv.* **2015**, *5*, 50421–50424.
[18]. Wang, J.; Li, Q.; Qi, C.; Liu, Y.; Ge, Z.; Li, R. Primary 1,2-diamine catalysis III: an unexpected domino reaction for the synthesis of multi substituted cyclohexa-1,3-dienamines. *Org. Biomol. Chem.* **2010**, *8*, 4240–4242.
[19]. Gaikwad, D. S.; Undale, K. A.; Patil, D. B.; Patravale, A. A.; Kamble, A. A. A task-specific biodegradable ionic liquid: a novel catalyst for synthesis of bicyclic ortho-aminocarbonitriles. *J. Iran. Chem. Soc.* **2018**, *15*, 1175–1180.
[20]. Lohar, T.; Kumbhar, A.; Barge, M.; Salunkhe, R. DABCO functionalized dicationic ionic liquid (DDIL): A novel green benchmark in multicomponent synthesis of heterocyclic scaffolds under sustainable reaction conditions. *J. Mol. Liq.* **2016**, *224*, 1102–1108.
[21]. Wan, Y.; Zhang, X.-X.; Zhao, L.-L.; Wang, C.; Chen, L.-F.; Liu, G.-X.; Huang, S.-Y.; Yue, S.-N.; Zhang, W.-L.; Wu, H. Tandem synthesis of bicyclicortho-aminocarbonitrile derivatives in ionic liquids: Tandem synthesis of bicyclicortho-aminocarbonitrile derivatives in ionic liquids. *J. Heterocycl. Chem.* **2015**, *52*, 623–627.
[22]. Wang, X.-S.; Wu, J.-R.; Zhou, J.; Zhang, M.-M. A green method for the synthesis of thiochromene derivatives in ionic liquids. *J. Heterocycl. Chem.* **2011**, *48*, 1056–1060.
[23]. Zhang, M.-M.; Wu, J.-R.; Zhou, J.; Wang, X.-S. Green method for the synthesis of polysubstituted chromene derivatives in ionic liquids. *Synth. Commun.* **2012**, *42*, 599–607.
[24]. Wehenkel, A.; Fernandez, P.; Bellinzoni, M.; Catherinot, V.; Barilone, N.; Labesse, G.; Jackson, M.; Alzari, P. M. The structure of PknB in complex with mitoxantrone, an ATP-competitive inhibitor, suggests a mode of protein kinase regulation in mycobacteria. *FEBS Lett.* **2006**, *580*, 3018–3022.
[25]. Chtita, S.; Aoumeur, N.; Belaidi, S.; Tchouar, N.; Ouassaf, M.; Lanez, T. Molecular docking studies for the identifications of novel antimicrobial compounds targeting of staphylococcus aureus. *Moroccan J. Chem.* **2021**, *9* (2), 274–289.
[26]. El-Feky, S. M.; Abou-Zeid, L. A.; Massoud, M. A.; Shokralla, S. G.; Eisa, H. M. Computational design, molecular modeling and synthesis of new 1,2,4 -triazole analogs with potential antifungal activities. *SMU Med. J.* **2014**, *1* (2), 224-242.
[27]. Jordá, T.; Puig, S. Regulation of ergosterol biosynthesis in Saccharomyces cerevisiae. *Genes (Basel)* **2020**, *11*, 795–795.
[28]. Azizi, N.; Ahooie, T. S.; Hashemi, M. M. Multicomponent domino reactions in deep eutectic solvent: An efficient strategy to synthesize multisubstituted cyclohexa-1,3-dienamines. *J. Mol. Liq.* **2017**, *246*, 221–224.
[29]. Sheldrick, G. M. A short history of SHELX. *Acta Crystallogr. A* **2008**, *64*, 112–122.
[30]. Spek, A. L. Structure validation in chemical crystallography. *Acta Crystallogr. D Biol. Crystallogr.* **2009**, *65*, 148–155.
[31]. Sheldrick, G. M. Crystal structure refinement with SHELXL. *Acta Crystallogr. C Struct. Chem.* **2015**, *71*, 3–8.
[32]. Wilson, A. J. C. International tables for crystallography. Volume C. corrigenda and addenda to the first edition. *Acta Crystallogr. A* **1995**, *51*, 441–444.
[33]. Macrae, C. F.; Bruno, I. J.; Chisholm, J. A.; Edgington, P. R.; McCabe, P.; Pidcock, E.; Rodriguez-Monge, L.; Taylor, R.; van de Streek, J.; Wood, P. A. Mercury CSD 2.0– new features for the visualization and investigation of crystal structures. *J. Appl. Crystallogr.* **2008**, *41*, 466–470.
[34]. Nardelli, M. PARST95 – an update to PARST: a system of Fortran routines for calculating molecular structure parameters from the results of crystal structure analyses. *J. Appl. Crystallogr.* **1995**, *28*, 659–659.
[35]. Frisch, M. J.; Trucks, G. W.; Schlegel, H. B.; Scuseria, G. E.; Robb, M. A.; Cheeseman, J. R.; Scalmani, G.; Barone, V.; Mennucci, B.; Petersson, G. A.; Nakatsuji, H.; Caricato, M.; Li, X.; Hratchian, H.P.; Izmaylov, A. F.; Bloino, J.; Zheng, G.; Sonnenberg, J. L.; Hada, M.; Ehara, M.; Toyota, K.; Fukuda, R.; Hasegawa, J.; Ishida, M.; Nakajima, T.; Honda, Y.; Kitao, O. ; Nakai, H.; Vreven, T.; Montgomery Jr., J. A.; Peralta, J. E.; Ogliaro, F. ; Bearpark, M.; Heyd, J. J.; Brothers, E.; Kudin, K. N.; Staroverov, V. N., Kobayashi, R.; Normand, J.; Raghavachari, K.; Rendell, A.; Burant, J. C.; Iyengar, S. S.; Tomasi, J.; Cossi, M.; Rega, N.; Millam, J. M.; Klene, M.; Knox, J. E.; Cross, J. B.; Bakken, V.; Adamo, C.; Jaramillo, J.; Gomperts, R.; Stratmann, R. E.; Yazyev, O.; Austin, A. J.; Cammi, R.; Pomelli, C.; Ochterski, J. W.; Martin, R. L.; Morokuma, K.; Zakrzewski, V. G.; Voth, G. A.; Salvador, P.; Dannenberg, J. J.; Dapprich, S.; Daniels, A. D.; Farkas, O.; Foresman, J. B.; Ortiz, J. V.; Cioslowski, J.; Fox, D. J. Gaussian 09, rev. A.01, Gaussian. Inc., Wallingford, CT, 2013.
[36]. Spackman, P. R.; Turner, M. J.; McKinnon, J. J.; Wolff, S. K.; Grimwood, D. J.; Jayatilaka, D.; Spackman, M. A. CrystalExplorer: a program for Hirshfeld surface analysis, visualization and quantitative analysis of molecular crystals. *J. Appl. Crystallogr.* **2021**, *54*, 1006–1011.
[37]. Trott, O.; Olson, A. J. AutoDock Vina: improving the speed and accuracy of docking with a new scoring function, efficient optimization, and multithreading. *J. Comput. Chem.* **2010**, *31*, 455–461.
[38]. Wang, X.-S.; Wu, J.-R.; Zhou, J.; Tu, S.-J. Green method for the synthesis of highly substituted cyclohexa-1,3-diene, polyhydroindene, polyhydronaphthalene, isochromene, isothiochromene, and isoquinoline derivatives in ionic liquids. *J. Comb. Chem.* **2009**, *11*, 1011–1022.
[39]. Zhang, L.-Z.; Wan, Y.; Zhang, X.-X.; Cui, H.; Zou, H.; Zhou, Q.-J.; Wu, H. Noncovalent catalysis of glucose-containing imidazolium salt in solvent-free one-pot synthesis of Ortho-aminocarbonitriles. *Tetrahedron Lett.* **2015**, *56*, 4934–4937.

[40]. Uzun, S.; Esen, Z.; Koç, E.; Usta, N. C.; Ceylan, M. Experimental and density functional theory (MEP, FMO, NLO, Fukui functions) and antibacterial activity studies on 2-amino-4- (4-nitrophenyl) -5,6-dihydrobenzo [h] quinoline-3-carbonitrile. *J. Mol. Struct.* **2019**, *1178*, 450–457.
[41]. Edwards, A. J.; Mackenzie, C. F.; Spackman, P. R.; Jayatilaka, D.; Spackman, M. A. Intermolecular interactions in molecular crystals: what's in a name? *Faraday Discuss.* **2017**, *203*, 93–112.
[42]. Murugavel, S.; Sundramoorthy, S.; Lakshmanan, D.; Subashini, R.; Pavan Kumar, P. Synthesis, crystal structure analysis, spectral (NMR, FT-IR, FT-Raman and UV–Vis) investigations, molecular docking studies, antimicrobial studies and quantum chemical calculations of a novel 4-chloro-8-methoxyquinoline-2(1H)-one: An effective anti microbial agent and an inhibition of DNA gyrase and lanosterol-14α-demethylase enzymes. *J. Mol. Struct.* **2017**, *1131*, 51–72.